

Role of Vanadyl Oxygen in Understanding Metallic Behavior of V₂O₅ (001) Nanorods

Raktima Basu, Arun K. Prasad, Sandip Dhara,* and A. Das*

Nanomaterials and Sensors Section, Surface and Nanoscience Division, Indira Gandhi Centre for Atomic Research, Homi Bhabha National Institute, Kalpakkam–603 102, India

Corresponding Authors

*Email Address: raktimabasu14@gmail.com; dhara@igcar.gov.in

Telephone: +91 44 27480015

Abstract

Vanadium pentoxide (V₂O₅), the most stable member of vanadium oxide family, exhibits interesting semiconductor to metal transition in the temperature range of 530-560K. The metallic behavior originates because of the reduction of V₂O₅ through oxygen vacancies. In the present report, V₂O₅ nanorods in the orthorhombic phase with crystal orientation of (001), are grown using vapor transport process. Among three non-equivalent oxygen atoms in a VO₅ pyramidal formula unit in V₂O₅ structure, the role of terminal vanadyl oxygen (O_I) in the formation of metallic phase above the transition temperature is established from the temperature dependent Raman spectroscopic studies. The origin of the metallic behavior of V₂O₅ is also understood due to the breakdown of *pdπ* bond between O_I and nearest V atom instigated by the formation of vanadyl O_I vacancy, confirmed from the downward shift of the bottom most split-off conduction bands in the material with increasing temperature.

1. Introduction

One dimensional transition metal oxides exhibit unique structure-property relationships which help in developing new electronic and photonic devices.^{1,2} Vanadium is a transition metal ($[\text{Ar}]3d^34s^2$) with multiple oxidation states leading to various stoichiometric oxides. Vanadium pentoxide (V_2O_5), which is essentially a semiconductor at room temperature, is the most stable form among them. Although, most of vanadium oxides such as VO_2 , V_2O_3 , V_6O_{13} exhibit metal to insulator transitions (MITs) as a function of temperature, in case of V_2O_5 it is quite contentious to use the term ‘MIT’.³ However, there are few reports about transition to metallic phase of V_2O_5 films around 530 to 553K and surface metallicity of (001) facet around 340 to 400K.⁴⁻⁶ The MIT is also reported to be reversible.⁶ The metallic behavior makes V_2O_5 applicable as gas sensors,^{7,8} thermochromic devices,^{9,10} optical and electrical switches¹¹ around the transition temperature.

The origin of the metallic behavior, however, is still not fully understood. The metallic transition was reported because of the reduction of V_2O_5 to other lower ordered stoichiometric or non-stoichiometric oxides without any structural change.^{5,12} In the structure of V_2O_5 there are three differently coordinated O atoms, namely, O_I (vanadyl), O_{II} (bridging), and O_{III} (chain) (schematic in the supplementary information Figure S1).¹³ There is also a dispute in the identification of the oxygen responsible for the reduction as all three O_I ,^{6,14} O_{II} ,¹⁵ and O_{III} ¹⁶ are suggested to be the eligible candidates. A structural phase transition from α - V_2O_5 to metastable γ' - V_2O_5 ,¹⁷ however, is also proposed with the increase in temperature to explain metallicity above the transition temperature, as γ' - V_2O_5 resembles conductive Wadsley phase of V_4O_9 .¹⁸

In the present study, we report semiconductor to metal transition of (001) oriented V_2O_5 nanorods, grown using vapour transport process. A transition from semiconducting to metallic

behavior was recorded in the temperature dependent I-V measurement. The reversible temperature dependent Raman spectra were analyzed for the allowed vibrational modes of semiconducting and metallic V_2O_5 phases to understand the origin of the transition. The change in electronic band structure after the reduction of V_2O_5 , prompting the metallicity in the sample, is discussed using temperature dependent Ultraviolet-Visible (UV-Vis) absorption spectroscopic studies and thermal activation energy calculations.

2. Experimental details

V_2O_5 nanorods were synthesized by vapor transport process using bulk VO_2 powder (Sigma-Aldrich, 99%) as source, placed in a high pure (99.99%) alumina boat at the center of the quartz tube reaction chamber, and flowing 20 sccm of Ar (99.9%) as carrier gas. Samples were grown on SiO_2/Si (100) using Au thin film (2 nm) as catalyst. The substrate was kept 5 cm away from the source normal to the stream of Ar. The synthesis was carried out at 1173K for 2 h.

Morphological analysis of the pristine sample was studied using a field emission scanning electron microscope (FESEM, SUPRA 55 Zeiss). The crystallographic studies were performed with the help of glancing incidence x-ray diffractometer (GIXRD; Bruker D8) using a $Cu K_\alpha$ radiation source ($\lambda=1.5406 \text{ \AA}$) with a glancing angle (θ) of 0.5° in the θ - 2θ mode. A micro-Raman spectrometer (inVia, Renishaw, UK), in the back scattering configuration, was used for Ar^+ laser (514.5 nm) excitation with a diffraction gratings of 1800 gr.mm^{-1} for monochromatization and a thermoelectric cooled charged coupled device (CCD) detector to study the vibrational modes. Electrical measurements were carried out by two Au coated contact tips. The activation energy E_a was calculated from the slope of $\ln(R)$ vs. $(1/T)$ plot, using the formula $R = R_0 \exp(-E_a/K_B T)$ where K_B is the Boltzmann constant, R_0 is the resistance at temperature $T=0K$. Absorption spectra were recorded using an UV-Vis absorption spectrometer

(Avantes) in the range of 200 to 700 nm. The Tauc's plots of the as-grown material, were drawn using $(\alpha h\nu)^{1/n}$ vs. $h\nu$ with $n = 2$ for indirect band gap semiconductor (absorption co-efficient, α ; Planck's constant, h ; frequency, ν). Temperature dependent spectroscopic studies and electrical measurements were performed in the Linkam (THMS600) stage.

3. Results and discussions

The typical field FESEM image (Figure 1(a)) of as-grown sample shows rod like structure with an average diameter of 200-300 nm. The inset in figure 1(a) shows high magnification image of a typical single nanorod.

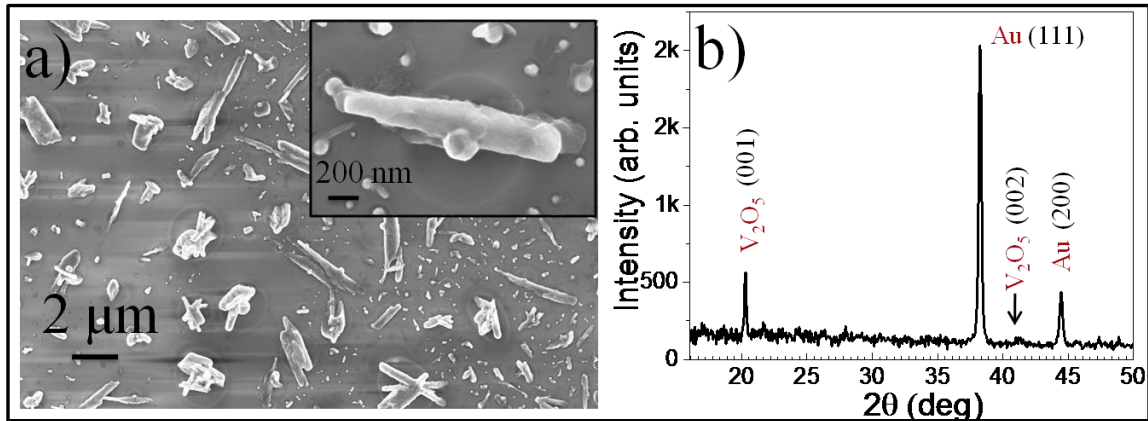


Figure 1. (a) FESEM image of as-grown nanorods. Inset shows a high resolution image of a typical nanorod (b) GIXRD spectrum of as-grown sample indicating crystalline planes corresponding to phases present.

The phase of the as-grown material was analyzed by GIXRD in the studies. Figure 1(b) shows the GIXRD data with peaks corresponding to the (hkl) planes of (001) and (002), confirming pure V₂O₅ phase (ICCD 00-041-1426) with unit cell dimensions $a = 11.51 \text{ \AA}$, $b = 3.56 \text{ \AA}$ and $c = 4.37 \text{ \AA}$ grown with (001) crystalline orientation.¹³ As we have used Au as catalyst

for the nanostructure growth, the GIXRD spectrum shows peaks corresponding to (111) and (200) planes for Au (ICCD 00-004-0784) also.

Group theoretical analysis predicts twenty one Raman active modes for V_2O_5 at Γ point, $7A_g+7B_{2g}+3B_{1g}+4B_{3g}$.¹⁹ However, we observed eleven Raman modes for as-grown nanorods (Figure 2), which match with the reported data for V_2O_5 .^{19,20}

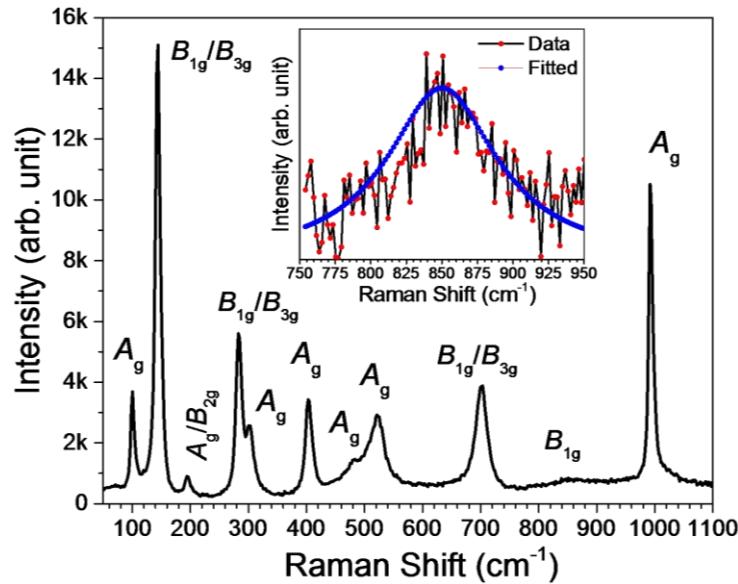


Figure 2. Raman spectrum of the as grown V_2O_5 nanorods with excitation of 514.5 nm at room temperature. The inset shows fitted peak at 850 cm^{-1} corresponding to B_{1g} mode.

The Raman peaks at 102 (A_g), 144 (either B_{1g} or B_{3g} ; B_{1g}/B_{3g}), 195 (A_g/B_{2g}), 283 (B_{1g}/B_{3g}), 301 (A_g), 403 (A_g), 483 (A_g), 523 (A_g), 701 (B_{1g}/B_{3g}), 850 (B_{1g}) and 993 (A_g) cm^{-1} confirm the presence of pure V_2O_5 phase.¹⁹ Orthorhombic V_2O_5 is made of distorted VO_5 pyramids sharing edges and corners having space group $P_{mmm} (D_{2h}^{13})$.²¹ The eleven observed Raman peaks can be assigned as follows. The highest frequency peak at 993 cm^{-1} appears due to the stretching vibrational mode of V-O_I bond along Z direction (detail structure may be referred to supplementary information Figure S1). The peak at 850 cm^{-1} (inset of Figure 2), observed

experimentally for the first time, is predicted to originate because of antiphase stretching mode of V-O_{II} bonds corresponding to the displacement of O_{II} atoms along *X* direction.¹⁹ The very weak intensity of the mode is due to pseudo-centrosymmetric nature of V-O_{II}-V bond.²⁰ Displacement of O_{III} atoms in *Y* and *X* directions generates Raman modes at 701 cm⁻¹ (V-O_{III}-V antiphase stretching mode) and 523 cm⁻¹ (*d*₄ stretching vibration), respectively. The V-O_{II}-V bending deformation along *Z* direction (*c* axis) gives rise to Raman mode at 483 cm⁻¹. Modes at 403 and 283 cm⁻¹ can be attributed to oscillation of O_I atoms along *X* and *Y* axes, respectively. On the other hand, displacement of O_{II} atoms along *Z* axis gives rise to Raman peak at 301 cm⁻¹. The low frequency modes at 195, 144 and 102 cm⁻¹ correspond to the *X*, *Y* and *Z* displacements of the whole chain involving shear and rotations of the ladder like V-O_{III} bonds.^{20,22} The high intensity of 144 cm⁻¹ peak indicates the long range order of V-O layers in the *XY* plane.²⁰

V₂O₅ is an indirect band gap semiconductor, with a gap value of about 2 eV.^{23,24} Presence of two localized narrow split-off bands with a gap of ~ 0.7 eV at the bottom of conduction band is considered as the most interesting feature of its electronic band structure.²⁴ The upper split-off band is separated from the main conduction band by an additional gap of 0.35 to 0.5 eV.²³⁻²⁵ However, V₂O₅ shows metallic behavior above the transition temperature.

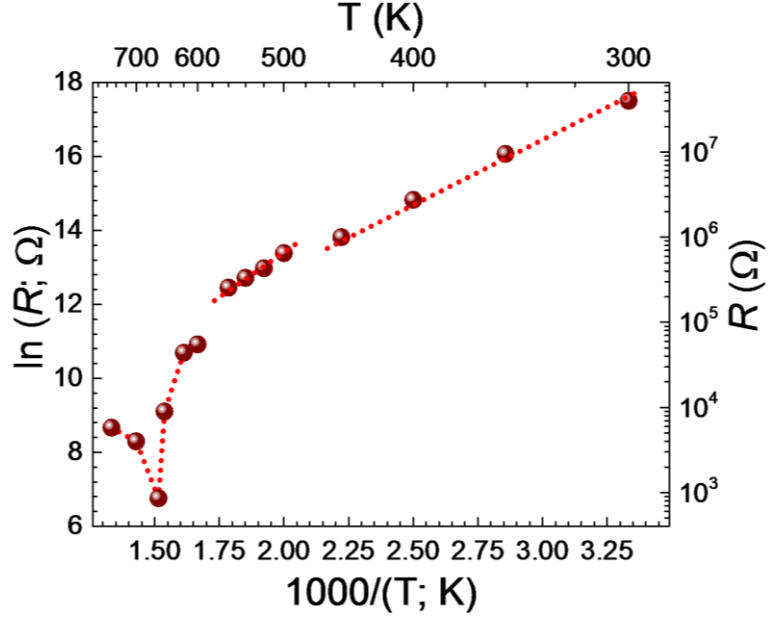


Figure 3. Change in the resistance with temperature in an ensemble of V_2O_5 nanorods

The semi log plot of resistance (R) vs. T^{-1} shows (Figure 3) that resistance decreases exponentially up to 450K with increasing temperature, indicating a semiconducting behavior leading to an activation energy of 0.29 ± 0.01 eV, which is slightly higher than the previously reported value (0.26 eV) for single crystalline V_2O_5 , measured in the temperature range of 200-270K.²⁶ The most possible reason for this low value of activation energy is due to the transition of electrons from localized split-off bands to main conduction band. In the temperature range of 500-550K, the slope of the plot is increased with an activation energy of 0.4 ± 0.01 eV, which indicates the downward shift of split-off bands with increasing temperature. Above 550K, it starts decreasing rapidly disobeying the semiconducting nature, and the plot shows metallic behavior of increasing resistance with increase in the temperature above 650K. As discussed earlier, the cause of the metallic behavior is still under debate.^{5,6,15-17} The proposed metallic phase of metastable γ' - V_2O_5 in the structural phase transition model,¹⁷ is reported to convert to a stable semiconducting α - V_2O_5 phase above 613K.²⁷ In the present study, however, the

temperature dependent electrical measurement shows (Figure 3) that the metallic character of the grown nanorods sustains above 650K, which contradicts the formation of γ' -V₂O₅. Hence the reduction of V₂O₅ through O vacancy with no structural change is likely in producing the metallic phase above the transition temperature.⁵ However, the role of specific O (supplementary information Figure S1) is still not clear in producing the metallic phase.

A temperature dependent Raman spectroscopic study (Figure 4(a)) was conducted to address the role of specific O in producing the metallic phase.

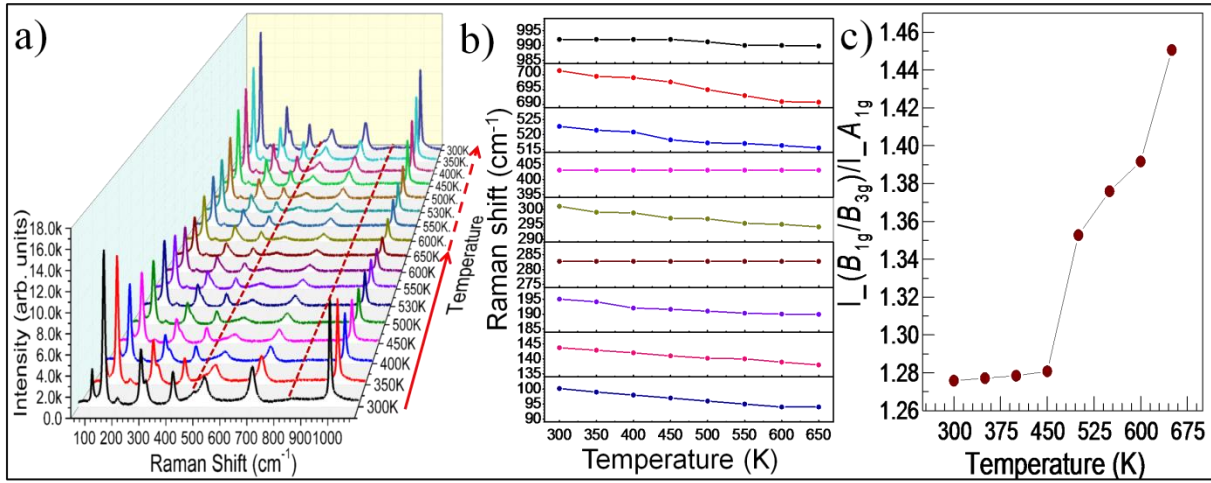


Figure 4. (a) Raman spectra of V₂O₅ nanorods with increasing (denoted by solid arrow) and decreasing (denoted by dashed arrow) temperature in the range of 300 to 650K (b) Change in vibrational frequency with temperature for each Raman mode and (c) Temperature dependence of the intensity ratio of the highest intense peak at 144 cm⁻¹ ($I_{(B_{1g}/B_{3g})}$) with the peak at 993 cm⁻¹ ($I_{(A_{1g})}$).

In temperature dependent Raman study, the modes at 483 and 850 cm⁻¹ are observed to disappear completely above the transition temperature of 530K and reappear again at the same temperature while cooling down. Moreover, a softening for all Raman modes was recorded with the increase in temperature except for the mode frequencies at 283, 403 and 993 cm⁻¹. Temperature

dependence (increasing) of frequencies for all the observed Raman modes is shown in figure 4(b). The peak positions of the Raman modes, except for the three above mentioned modes, are red shifted by an amount of 7 to 13 cm^{-1} in the temperature range from 300 to 650K. The intensity of the peak centered at 993 cm^{-1} is observed to decrease rapidly with the increase in temperature and regain almost its original intensity after cooling back to room temperature. The intensity ratio of the highest intense 144 cm^{-1} (B_{1g}/B_{3g}) Raman mode with 993 cm^{-1} (A_{1g}) mode with increasing temperature is shown in figure 4(c). The intensity ratio ($I_{(B_{1g}/B_{3g})}/I_{A_{1g}}$) increases rapidly above the temperature 450K indicating a significant decrease in the intensity of A_{1g} mode centered at 993 cm^{-1} as compared to that of B_{1g}/B_{3g} mode of 144 cm^{-1} around the transition temperature of 530K. The drastic fall in intensity of the A_{1g} mode, which is responsible for the vibration of vanadyl O_I atoms along c -axis alone, signifies the possible loss of O_I atoms from the structure around the transition temperature. It may also be noted that the B_{1g}/B_{3g} mode frequency at 144 cm^{-1} is independent of the motion of O_I , so our inference about the role of O_I influencing the intensity of A_{1g} mode at 993 cm^{-1} is mutually exclusive. Moreover, it is reported that the vanadyl O_I is more prone to reduction, as the vacancy formation energy is lower for O_I atoms than the other two coordinated oxygen atoms (O_{II} and O_{III}) in V_2O_5 (001) oriented surface.^{28,29} The modes at 483 and 850 cm^{-1} , arising due to V- O_{II} -V bending and stretching vibrations, respectively, disappeared above the transition temperature. It may be due to the relaxation of V_2O_5 structure initiated with the formation of vanadyl O_I vacancy (schematic in the supplementary information Figure S2). If one of the vanadyl oxygen atoms are removed from the surface, the V atom in its near vicinity projects inward for relaxation and the next right vanadyl oxygen relax upward to make a stiffer interlayer bond with increased bond length (1.78 Å). Moreover, the V- O_{II} -V bond angle is also reported to increase to 178° leading to almost a linear

bond.²⁸ So, the disappearance of the modes at 483 and 850 cm^{-1} is in quite good agreement with the relaxation conditions. The absence of phonon softening with temperature for the Raman modes at 283, 403 and 993 cm^{-1} , which originates due to the *Y*, *X* and *Z* vibration of O_I atoms, respectively, may also be attributed to the structural relaxation as the V- O_I bonds become stiffer between the layers after the relaxation. The reversibility of the Raman modes with temperature can be explained by the excellent catalytic behavior of V_2O_5 . Structural phase transition to γ' - V_2O_5 is further ruled out with the absence of Raman mode at 602 cm^{-1} ,³⁰ in the studied temperature range of 300-650K.

To understand the origin of metallicity in V_2O_5 , temperature dependent UV-Vis absorption of the as-grown V_2O_5 nanorods was studied. V_2O_5 is a semiconductor with an indirect band gap of ~ 2 eV corresponding to a transition from *R* to Γ point in the first Brillouin zone.^{23,24} Two split-off bands with narrow bandwidth (0.45 to 0.75 eV) below the conduction band at Γ point are also reported.^{24,25} Vanadyl O_I plays an important role in creating these split-off conduction bands.^{31,32} The Tauc's plot of the as-grown material, using $(\alpha h\nu)^{1/2}$ vs. $h\nu$ for indirect band gap semiconductor (absorption co-efficient, α ; Planck's constant, h ; frequency, ν), at different temperatures ranging from 300 to 650K are shown in figure 5.

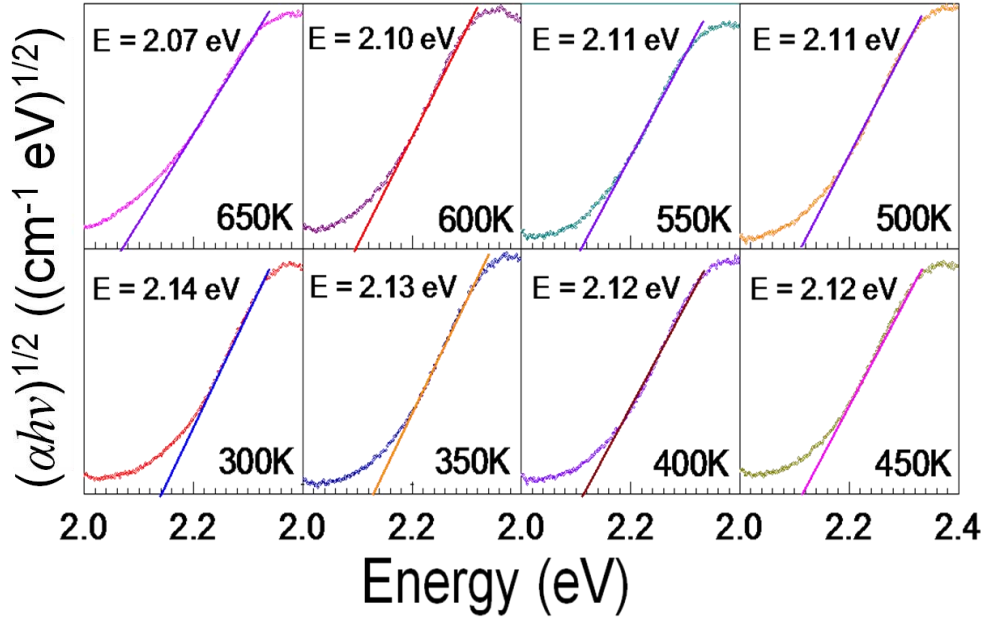


Figure 5. Tauc's plot of indirect band gap V_2O_5 nanorods using UV-Visible spectra at different temperatures. The slopes are drawn to determine the band gap value, as inscribed in the insets for the plots at different temperatures.

An indirect band gap of 2.14 eV, which matches with the previously reported value of 2.1 eV,³³ was recorded at 300 K. The band gap decreases with increase in temperature and is measured to attain a value of 2.07 eV at 650K. The decrease in band gap by an amount of 70 meV indicates downward shift of the split-off bands with increase in temperature, as also inferred from the thermal activation energy analysis (Figure 3). Inspired by the vanadyl O_1 vacancy, the split-off conduction bands are reported to approach deeper down from the conduction band at Γ point due to the breakdown of $pd\pi$ bond between O_1 and nearest V atom.^{14,31,32} Reduction of an oxygen atom donates two electrons back to the structure. The breakdown of $pd\pi$ bond between O_1 and nearest V atom results in delocalization of electrons towards neighboring V cation by occupying the partially filled V $3d$ states in the conduction band,³⁴ leading to the increase in the number of carriers in the conduction band. The increased number of carriers in the conduction band may be

responsible for the decrease in resistance above the transition temperature and the observed metallic behavior. Thus, the decrease in band gap with increasing temperature supports our assumption of vanadyl O_I vacancy from the V₂O₅ structure above the transition temperature.

3. Conclusion

In conclusion, orthorhombic V₂O₅ (001) nanorods were synthesized by vapor transport method. Temperature dependent electrical properties showed a transition of semiconducting to metallic behavior at temperature of 550K. Phonon softening behavior in the temperature dependent Raman spectra indicated loss of vanadyl oxygen (O_I) as the most possible reason for the observation of the metallic V₂O₅ phase above the transition temperature. Reduction of the band gap with increasing temperature, as observed in the Tauc's plot and thermal activation energy calculations, implies the downward movement of split-off bands from the conduction band. The downward shift of split-off bands with increase in temperature is due to breakdown of *pdπ* bond between O_I and nearest V atom, inspired by the formation of vanadyl O_I vacancy. The breakdown of *pdπ* bonds helps in accumulating electrons towards neighboring V atom to occupy the partially filled V 3*d* bands, leading to the increase in the number of carriers in conduction band, which is finally made responsible for the decrease in the resistance and the observed metallic behavior, for the first time.

AUTHOR INFORMATION:

*Email Address: raktimabasu14@gmail.com; dhara@igcar.gov.in

ACKNOWLEDGMENT

One of us (RB) thanks DAE, India for financial support. We also acknowledge D. N. Sunitha, S. R. Polaki and A. Pasta of SND, IGCAR for their help in GIXRD, FESEM and electrical studies, respectively.

REFERENCES

- (1) Poizot, P.; Laruelle, S.; Grugeon, S.; Dupont, L.; Tarascon, J-M. Nano-Sized Transition Metal Oxides as Negative-Electrode Materials for Lithium-Ion Batteries. *Nature* **2000**, *407*, 496-499.
- (2) Rao, C.N. R. Transition Metal Oxides. *Annu. Rev. Phys. Chem.* **1989**, *40*, 291-326.
- (3) Pergament, A.; Stefanovich, G.; Andreev, V. Comment on “Metal-Insulator Transition without Structural Phase Transition in V₂O₅ Film” [Appl. Phys. Lett. 98, 131907 (2011)] *Appl. Phys. Lett.* **2013**, *102*, 176101.
- (4) Nadkarni G. S.; Shirodkar, V. S. Experiment and Theory for Switching in Al/V₂O₅/Al Devices. *Thin solid films* **1983**, *105*, 115-129.
- (5) Kang, M.; Kim, I.; Kim, S. W.; Ryu, J.-W.; Park, H. Y. Metal-Insulator Transition without Structural Phase Transition in V₂O₅ Film. *Appl. Phys. Lett.* **2011**, *98*, 131907-3.
- (6) Blum, R. -P.; Niehus, H.; Hucho, C.; Fortrie, R.; Ganduglia-Pirovano, M. V.; Sauer, J.; Shaikhutdinov, S.; Freund, H.-J. Surface Metal-Insulator Transition on a Vanadium Pentoxide (001) Single Crystal. *Phys. Rev. Lett.* **2007**, *9*, 226103-4.
- (7) Raible, I.; Burghard, M.; Schlecht, U.; Yasuda, A.; Vossmeier, T. V₂O₅ Nanofibres: Novel Gas Sensors with Extremely High Sensitivity and Selectivity to Amines. *Sens. Actuators B* **2005**, *106*, 730-735.
- (8) Dhayal Raj, A.; Pazhanivel, T.; Kumar, P. S.; Mangalaraj, D.; Nataraj, D.; Ponpandian, N. Self Assembled V₂O₅ Nanorods for Gas Sensors. *Curr. Appl. Phys.* **2010**, *10*, 531-537.
- (9) Nishio, S.; Kakihana, M. Evidence for Visible Light Photochromism of V₂O₅. *Chem. Mater.* **2002**, *14*, 3730-3733.

- (10) Zuli, L.; Guojia, F.; Youqing, W.; Yandong, B. Laser-Induced Colouration of V₂O₅. *J. Phys. D: Appl. Phys.* **2000**, *33*, 2327-2332.
- (11) Krishnakumar, S.; Menon, C. S. Optical and Electrical Properties of Vanadium Pentoxide Thin Films. *phys. stat. sol. (a)* **1996**, *153*, 439-444.
- (12) Xie, S.; Iglesia, E.; Bell, A. T. Effects of Temperature on the Raman Spectra and Dispersed Oxides. *J. Phys. Chem. B* **2001**, *105*, 5144-5152.
- (13) Enjalbert, R.; Galy, J. A Refinement of the Structure of V₂O₅. *Acta Crystallogr., Sect. C: Cryst. Struct. Commun.* **1986**, *42*, 1467-1469.
- (14) Lambrecht, W.; Djafari-Rouhani, B.; Vennik, J. Electronic Structure of Bulk and Surface Vanadyl Oxygen Vacancies in the Layer Compound V₂O₅. *Surf. Sci.* **1983**, *126*, 558-564.
- (15) Eon, J. G.; Olier R.; Volta, J. C. Oxidative Dehydrogenation of Propane on γ -Al₂O₃ Supported Vanadium Oxides. *J. Catal.* **1994**, *145*, 318-326.
- (16) Ramirez, R.; Casal, B.; Utrera, L.; Ruiz-Hitzky, E. Oxygen Reactivity in Vanadium Pentoxide: Electronic Structure and Infrared Spectroscopy Studies. *J. Phys. Chem.* **1990**, *94*, 8960-8965.
- (17) Rubin Aita, C. Additional Comment on “Metal-Insulator Transition without Structural Phase Transition in V₂O₅ Film” [Appl. Phys. Lett. 98, 131907 (2011)]. *Appl. Phys. Lett.* **2014**, *104*, 176101-2.
- (18) Wilhelmi, K. A.; Walterson, K. On the Crystal Structure of a New Vanadium Oxide, V₄O₉. *Acta. Chem. Scand.* **1970**, *24*, 3409-3411.
- (19) Abello, L.; Husson, E.; Repelin, Y.; Lucazeau, G. Vibrational Spectra and Valence Force Field of Crystalline V₂O₅. *Spectrochim. Acta, Part A: Mol. Spectrosc.* **1983**, *39*, 641-651.

- (20) Baddour-Hadjean, R.; Pereira-Ramos, J. P.; Navone, C.; Smirnov, M. Raman Microspectrometry Study of Electrochemical Lithium Intercalation into Sputtered Crystalline V_2O_5 Thin Films. *Chem. Mater.* **2008**, *20*, 1916-1923.
- (21) Bachmann, H. G.; Ahmed, F. R.; Barnes, W. H. The Crystal Structure of Vanadium Pentoxide. *Z. Kristallogr.* **1961**, *115*, 110-131.
- (22) Clauws, P.; Broeckx, J.; Vennik, J. Lattice Vibrations of V_2O_5 . Calculation of Normal Vibrations in a Urey-Bradley Force Field. *phys. stat. sol. (b)* **1985**, *131*, 459-473.
- (23) Chakrabarti, A.; Hermann, K.; Druzinic, R.; Witko, M.; Wagner, F.; Petersen, M. Geometric and Electronic Structure of Vanadium Pentoxide: A Density Functional Bulk and Surface Study. *Phys. Rev. B* **1999**, *59*, 10583-10590.
- (24) Parker, J. C.; Lam, D. J.; Xu, Y.-N.; Ching, W. Y. Optical properties of vanadium pentoxide determined from ellipsometry and band-structure calculations. *Phys. Rev. B* **1990**, *42*, 5289-5293.
- (25) Eyert V.; Höck, K.-H. Electronic Structure of V_2O_5 : Role of Octahedral Deformations. *Phys. Rev. B* **1998**, *57*, 12727-12737.
- (26) Karakotsou, Ch.; Kalomiros, J. A.; Hantias, M. P.; Anagnostopoulos, A. N.; Spyridelis, J. Nonlinear Electrical Conductivity of V_2O_5 Single Crystals. *Phys. Rev. B* **1992**, *45*, 11627-11631.
- (27) Cocciantelli, J. M.; Gravereau, P.; Doumerc, J. P.; Pouchard, M.; Hagenmuller, P. On the Preparation and Characterization of a New Polymorph of V_2O_5 . *J. Solid State Chem.* **1991**, *93*, 497-502.
- (28) Ganduglia-Pirovano, M.; Sauer, J. Stability of Reduced V_2O_5 (001) Surfaces. *Phys. Rev. B* **2004**, *70*, 045422-13.

- (29) Sauer, J.; Dobler, J. Structure and Reactivity of V₂O₅: Bulk Solid, Nanosized Clusters, Species Supported on Silica and Alumina, Cluster Cations and Anions. *Dalton Trans.* **2004**, 3116-3121.
- (30) Baddour-Hadjean, R.; Smirnov, M. B.; Kazimirov, V. Y.; Smirnov, K. S.; Pereira-Ramos, J.-P. The Raman Spectrum of the Γ' -V₂O₅ Polymorph: A Combined Experimental and DFT Study. *J. Raman Spectrosc.* **2015**, *46*, 406-412.
- (31) Lambrecht, W.; Djafari-Rouhani, B.; Vennik, J. On the Origin of the Split-Off Conduction Bands in V₂O₅. *J. Phys. C: Solid State Phys.* **1981**, *14*, 4785-4795.
- (32) Lambrecht, W.; Djafari-Rouhani, B.; Vennik, J. Theoretical Study of the Vanadyl-Oxygen Vacancy in V₂O₅: Tight-Binding Green Function Calculation, Optical Properties and Neutral Vacancy Ground-State Splitting. *J. Phys. C: Solid State Phys.* **1986**, *19*, 369-388.
- (33) Khan, G. A.; Hogarth, C. A.; Electron Spin Resonance Studies of Evaporated V₂O₅ and Co-Evaporated V₂O₅/B₂O₃ Thin Films. *J. Mater. Sci.* **1991**, *26*, 2707-2710.
- (34) Wu, Q.-H.; Thissen, A.; Jaegermann, W.; Liu, M. Photoelectron Spectroscopy Study of Oxygen Vacancy on Vanadium Oxides Surface. *Appl. Surf. Sci.* **2004**, *236*, 473-478.

Supplementary information

Role of Vanadyl Oxygen in Understanding Metallic Behavior of V_2O_5 (001) Nanorods

Raktima Basu,* Arun K. Prasad, Sandip Dhara,* and A. Das

Nanomaterials and Sensors Section, Surface and Nanoscience Division, Indira Gandhi Centre for Atomic Research, Homi Bhabha National Institute, Kalpakkam–603 102, India

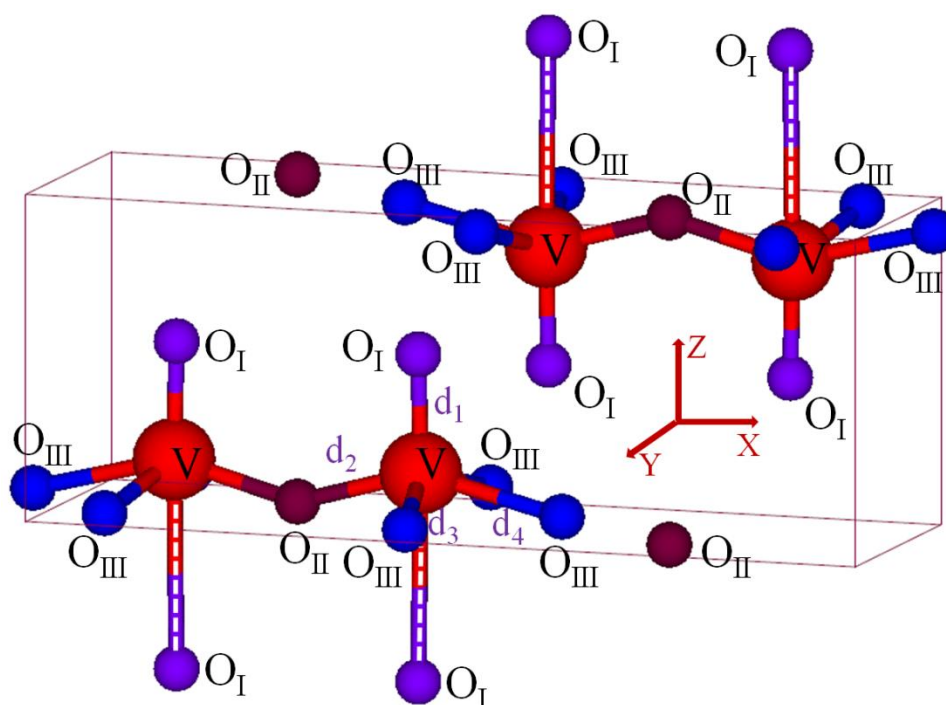


Figure S1. Schematic diagram of V_2O_5 unit cell

Figure S1 shows the schematic diagram of V_2O_5 unit cell. Orthorhombic V_2O_5 crystallizes in a layered structure perpendicular to the Z-axis consisting of VO_5 pyramids sharing their vertices and corners. There are three non-equivalent oxygen atoms in each unit cell (denoted as O_I , O_{II} , and O_{III}). O_I is the terminal (vanadyl) oxygen with two different bond lengths. One of them is strong and short V- O_I bond with length 1.577 Å (d_1). Another one is large and weak Van der Waals type, which connects the two adjacent layers in the V_2O_5 structure, with a bond length of 2.793 Å (shown by dotted white lines). Both of these vanadyl oxygen atoms orient almost along the c-axis. The two fold coordinated bridging oxygen (O_{II})

connects two adjacent V atoms with V-O_{II} bond length of 1.78 Å (d_2). The ladder shaped O_{III} atoms are the three-fold coordinated oxygen with three different V-O_{III} bond lengths of 1.88 (d_3), 1.88 (d_3), and 2.02 Å (d_4) [Ref: 13 in the main text].

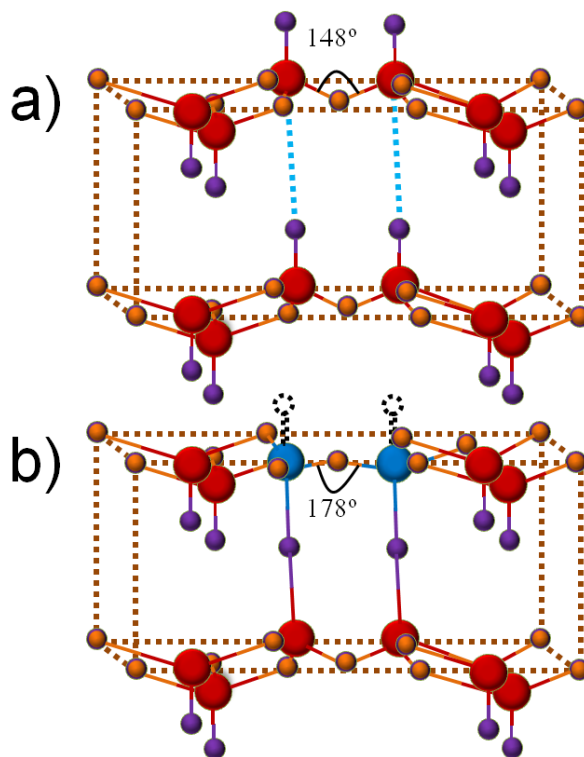


Figure S2. Schematic diagram of V₂O₅ unit cell (a) below and (b) above transition temperature

Figure S2 shows the structure of V₂O₅ unit cell below (Figure S2 (a)) and above (Figure S2 (b)) the transition temperature. If one of the vanadyl oxygen atoms are removed from the surface, the V atom in its near vicinity projects inward for relaxation and the next right vanadyl oxygen relax upward to make a stiffer interlayer bond with increased bond length (1.78 Å). Moreover, the V-O_{II}-V bond angle is also reported to increase to 178° leading to almost a linear bond. [Ref: 28 in the main text].